Chapter 6

CORONAL MAGNETIC FIELD MEASUREMENTS THROUGH BREMSSTRAHLUNG EMISSION

G.B.Gelfreikh
Central (Pulkovo) Astronomical Observatory RAS. St.Petersburg 196140, Russia
GBG@GG1623.spb.edu

Abstract Basic concepts are presented of the theory of thermal bremsstrahlung in the anisotropic plasma of the solar atmosphere. Formulas are given describing the polarization resulting from the solar magnetic field, from which the longitudinal component of the magnetic field can be found through analysis of the polarization spectra of the thermal radio emission. The application of the method is illustrated with examples pertaining to solar faculae, prominences, coronal holes and coronal loops. The observations were carried with large, modern radio telescopes such as the Nobeyama Radioheliograph (Japan) and the RATAN-600 (Russia).

1. Introduction

Many forms of electromagnetic emission arise as a result of the acceleration of charged particles. In the case under consideration here, the acceleration is caused by the electrostatic field of ions and the emitting particles are electrons. In some approximation this process may be considered as particle collisions. This mechanism is usually called bremsstrahlung, although the term free-free emission is also used in the astrophysical literature. In fact, this mechanism for generating radio emission may be considered the main one produced by a thermal plasma (e.g. see Benz 1993), since it is always present.

2. Basic Formulae

2.1 Equations of transfer of the thermal emission in anisotropic plasma

For the intensity of the emission we have the equation of transfer:

$$I(\nu) = \int \eta(l)\, e^{-\tau(l)}\, dl, \tag{6.1}$$

where the emissivity $\eta(\nu)$ is the energy emitted per unit volume per unit solid angle per unit interval of the wave frequency ν. Absorption coefficient $\kappa(\nu)$ is the relative decrease of intensity per unit length of the ray. The optical thickness is the integral of κ along the ray path:

$$\tau = \int \kappa(l)\, dl. \tag{6.2}$$

If the emitting particles have a thermal distribution (that is, have Boltzmann's distribution in energy space, or Maxwell's distribution in velocity space) then the emissivity η and absorption coefficient κ are connected by a simple relation (Kirchhoff's law)

$$\frac{\eta}{\kappa} = B(T) = \frac{2kT}{\lambda^2} = \frac{2kT\nu^2}{c^2}, \tag{6.3}$$

where $B(T)$ is the Planck function. The Rayleigh-Jeans approximation to the Planck function (valid in the radio regime) has been used in the above equation.

For observations in the radio wave range the intensity usually is given in units of brightness temperature defined by the relation

$$I = \frac{2kT_b}{\lambda^2} = \frac{2kT_b\nu^2}{c^2}. \tag{6.4}$$

This implies that the brightness temperature T_b is equal to the temperature of the black body producing the same intensity (or having the same brightness). In these terms the equation of transfer has the form

$$T_b = \int T(\tau) e^{-\tau} d\tau. \tag{6.5}$$

The values η and κ are also functions of plasma parameters such as

- electron density n_e and/or of other particles n_i (ions and neutral particles);
- electron temperature T_e;
- magnetic field $\mathbf{B}$, its strength and direction.

In magneto-ionic theory, when the approximation of geometrical optics is valid, two types of waves—called the ordinary and extraordinary modes—can propagate in a plasma. They correspond approximately to the two orthogonal circular polarizations. Thus, in an anisotropic (i.e. magnetized) plasma we must write two separate equations of transfer for ordinary (o) and extraordinary (x) modes:

$$\begin{aligned} T_b^o &= \int T(\tau^o)\, e^{-\tau^o}\, d\tau^o \\ T_b^x &= \int T(\tau^x)\, e^{-\tau^x}\, d\tau^x. \end{aligned} \tag{6.6}$$

In most cases we treat these "normal modes" as left-handed and right-handed circular polarization.

We should keep in mind that $T_b(\nu)$ is also a function of temperature, density, magnetic field and other plasma parameters in the region of generation and propagation of the electromagnetic waves. The goal of plasma diagnostics is the evaluation of these parameters. To get these we deal with the solution of the equations of the form:

$$F(T, n_e, \mathbf{B}, \dots) = T_b(\nu). \tag{6.7}$$

In general, even with high-resolution imaging, the values n_e, $\mathbf{B}$, T, etc., that we wish to find are in fact averaged along the line of sight at some position in the object of study.

2.2 Basic expression for the case of the isotropic plasma

For the absorption coefficient in isotropic plasma we can use the expression

$$\kappa = \frac{\zeta n_e^2}{T^{3/2}\nu^2}, \tag{6.8}$$

which is a simplification of the full expression (4.6) given in Chapter 4. The coefficient ζ only slightly (logarithmically) depends on the plasma parameters. In most cases of solar interest, its value is within the range 0.12–0.2. In the following discussion we will consider it a constant. Generally speaking, in determining the value of ζ the chemical composition and degree of ionization of the plasma must be taken into account.

Since we here consider only the case of thermal emission, we can use Kirchhoff's law to evaluate the expression for the emissivity using (6.8):

$$\eta = \frac{2\zeta k}{c^2}\frac{n_e^2}{\sqrt{T}}. \tag{6.9}$$

2.3 Basic expression for the case of anisotropic plasma

Now we present the expressions for the absorption coefficient for an anisotropic plasma in the presence of a magnetic field $\mathbf{B}_0$. In this case the absorption coefficient becomes:

$$\kappa_{o,x} = \frac{\zeta n_e^2}{T^{3/2}(\nu \pm \nu_B|\cos\alpha|)^2}, \tag{6.10}$$

where ν_B is the electron gyrofrequency. For the two types of the circular polarization of normal modes

$$\kappa_{L,R} = \frac{\zeta n_e^2}{T^{3/2}(\nu \pm \nu_B \cos\alpha)^2}. \tag{6.11}$$

In all equations above we assume that the refractive index $\tilde{n} = 1$. This can be checked if necessary using the expression

$$\tilde{n}^2 = 1 - \frac{\nu_p^2}{\nu^2} = 1 - \frac{n_e e^2}{\pi m_e \nu^2}, \tag{6.12}$$

where m_e and e are the mass and charge of an electron.

3. Diagnostics of the Coronal Plasma

The central point of our discussion here is to measure the magnetic field using spectral-polarization observations of the radio bremsstrahlung of the thermal plasma. One of the serious problems of the method is identification of the mechanism generating the observed structure on the radio map of the Sun.

3.1 Diagnostics of the mechanism of the emission generated by thermal bremsstrahlung

From the frequency dependence of opacity given by (6.8), the equation of transfer (6.1) can be analyzed with the known spectral index for optical depth:

$$\tau(\lambda) \propto \lambda^2. \tag{6.13}$$

At the same time, to a good approximation the emissivity, η, in (6.9) does not depend on the wavelength λ (or frequency ν). And so, it follows that

$$\frac{\partial I}{\partial \lambda} \leq 0. \tag{6.14}$$

For shorter wavelengths, where $\tau \ll 1$

$$I(\lambda) = const. \tag{6.15}$$

This flat flux density spectrum is an important characteristic of bremsstrahlung by which to identify the radio emission mechanism. Another important property is the limit in brightness temperature to be expected of thermal emission:

$$T_b \leq T_e, \tag{6.16}$$

where T_e is the electron temperature. If the emission mechanism is thermal bremsstrahlung, then the brightness temperature must not exceed reasonable

values of the electron temperature for the plasma. The value of T_e refers to some point in the emitting plasma structure. For the case of optically thick regions a reasonable approximation is

$$T_b(\lambda) = T_e \qquad (\tau(\lambda) \geq 1) \tag{6.17}$$

We shall refer to this condition later. We should also notice that κ and especially η depend strongly on electron density and inversely on temperature (see 6.8 and 6.9). Thus, observations of bremsstrahlung are most effective in the denser, cooler regions of the solar atmosphere.

So far in the diagnostics of the mechanism of thermal bremsstrahlung we have used expressions for isotropic plasma. However in reasonably good approximation this assumption works also for anisotropic plasma if the magnetic fields are not too strong.

3.2 Expressions for the magnetic field

Now, once we have come to the conclusion that the mechanism responsible for the observed radio emission is indeed thermal bremsstrahlung, from analysis of its intensity (brightness) spectrum, the next step is to analyze its polarization—the main source of information on the magnetic field within the source. The analysis is based on the equations of transfer for an anisotropic plasma (6.6), from which we can derive the equation giving the strength of the magnetic field in the source region generating the thermal bremsstrahlung.

We define the degree of polarization as

$$P = \frac{T_b^R - T_b^L}{T_b^R + T_b^L}, \tag{6.18}$$

where the brightness temperatures for the two types of the circular polarization as a function of the wavelength λ are to be determined by the equations of transfer (6.6). Optical thickness $\tau^{R,L}$ is found using (6.10) and (6.11). For the case of the optically thin region we have, to a good approximation,

$$T_b^{x,o} = T_e \, \tau_{x,o} \qquad (\tau \ll 1), \tag{6.19}$$

or

$$T_b^{L,R} = T_e \, \tau_{L,R} \, . \tag{6.20}$$

Then follows

$$P = \frac{T_b^x - T_b^o}{T_b^x + T_b^o} = \frac{\tau_x - \tau_o}{\tau_x + \tau_o} \approx 2\frac{\nu_B}{\nu} |\cos\alpha| \, , \tag{6.21}$$

or, taking into account the sign of polarization,

$$P = \frac{T_b^R - T_b^L}{T_b^R + T_b^L} = \frac{\tau_R - \tau_L}{\tau_R + \tau_L} = 2\frac{\nu_B}{\nu}\cos\alpha \ . \tag{6.22}$$

In the case of optically thick plasma the brightness temperature is $T_b = T_e$ — some (density weighted) mean value of the electron temperature along the line of sight. For isothermal plasma

$$T_b^x = T_b^o = T_e \tag{6.23}$$

and $P = 0$ —no polarization is observed and no magnetic field measurements are possible. The existence of a gradient in temperature with height, however, changes the situation. The optical thickness for ordinary mode $\tau^o < \tau^x$ for extraordinary mode and so we look into deeper, usually colder, layers of the solar atmosphere. The resulting equation for polarization can be found from the equations of transfer using the approximation of the weak magnetic field:

$$P = n\frac{\nu_B}{\nu} \mid \cos\alpha \mid \ . \tag{6.24}$$

Here spectral index n is given by the equation

$$n \equiv -\frac{\partial(\log T_b)}{\partial(\log\nu)} = \frac{\partial(\log T_b)}{\partial(\log\lambda)} \ , \tag{6.25}$$

and can be measured directly from spatially resolved spectral observations. If the sign of polarization is taken into account, then instead of (6.24) we have

$$P = n\frac{\nu_B}{\nu}\cos\alpha \ . \tag{6.26}$$

Recalling that the electron gyrofrequency is $\nu_B = 2.8 \times 10^6 B$, and noting that $B\cos\alpha = B_l$ is the longitudinal component of the magnetic field, (6.26) becomes

$$P = n\frac{2.8 \times 10^6}{\nu}B_l \ . \tag{6.27}$$

3.3 Radio measurements of the magnetic field

These expressions may be successfully used to measure the longitudinal component of magnetic fields in the solar atmosphere, keeping in mind that they refer to an average over the line of sight, weighted by n_e^2 and $T_e^{-3/2}$. To this end it is reasonable to write them in terms of the strength of the longitudinal component of the magnetic field. For the optically thin region, where we expect the spectral slope $n = 2$, we have

$$B_l = \frac{54}{\lambda}P\% \ . \tag{6.28}$$

In this case the longitudinal component of the magnetic field B_l can be found from observations at one wavelength. In fact, however, spectral observations in this case are also necessary to confirm the bremsstrahlung nature of the radio emission and that we really deal with an isolated optically thin region (for example as viewed above the solar limb).

The longitudinal component of the magnetic field in the more general situation may be written in the form

$$B_l = \frac{107}{\lambda \cdot n} P\% \, . \tag{6.29}$$

Both $P\%$ and n can be found from observations. So, we have come to a viable method of performing radio magnetography, provided $P\%$ and n can be measured with sufficient precision.

4. Expected Parameters of Polarized Radio Emission from the Solar Plasma

Using (6.29), we can measure the longitudinal component of the magnetic field both in the solar corona and upper chromosphere, including the transition region. The method is applicable, both on the disk and above the solar limb, to most plasma structures in the upper solar atmosphere that are organized by sufficiently strong local magnetic fields. Such fields are not easily accessible to traditional optical methods, such as Zeeman splitting of spectral lines or the Hanlé effect, except in special cases. Infrared techniques are currently being developed which may provide Zeeman measurements above the limb.

4.1 Optically thin regions

According to (6.13), (6.20) and (6.21) we have in this case

$$\begin{array}{lll} T_b & \propto & \lambda^2 \\ P & \propto & \lambda \end{array} \tag{6.30}$$

It follows that the sensitivity to the magnetic field increases with the wavelength λ. However, at the same time the optical depth of coronal structures increases for longer wavelengths and so weakens the polarization. Another important limitation in applicability of the method is the possible simultaneous presence of other radio emission mechanisms typical for the solar active regions. The central role here belongs to the thermal cyclotron (gyroresonance) emission (see Chapter 5). This mechanism becomes effective at frequencies corresponding typically to the third harmonic of the electron gyrofrequency. In this case, the magnetic field can be estimated according to the equation

$$B(\nu = 3\nu_B) = \frac{3570}{\lambda(\mathrm{cm})} = 119 \, \nu_{\mathrm{GHz}} \, . \tag{6.31}$$

While for the sunspots this kind of radio emission is usually important at wavelengths $\gtrsim 2$ cm, for the weaker fields elsewhere in the active region it may be important from $\gtrsim 5$ cm. These sources are identified by strong polarization and high brightness, and so can be excluded from the analysis of thermal bremsstrahlung.

One may conclude that the study of magnetic fields with thermal bremsstrahlung complements their study via the gyroresonance mechanism. Thermal bremsstrahlung can be used in coronal structures and parts of ARs where the magnetic field is weaker than 100–200 G, where the radio brightness and degree of polarization are rather low. The coronal condensations (increases in density) can be studied both behind the limb and on the disk. With the sensitivity of, say 0.1% at $\lambda = 5$ cm, we achieve the sensitivity in the coronal magnetic fields of about 1 G. This high precision is not easy to achieve with present techniques but, on the other hand, there are no principal limitations to its achievement.

4.2 Optically thick regions

In the case $\tau \gg 1$ the polarization is determined by the gradient of temperature in the emitting layers of the solar atmosphere. A good approximation for the short cm and mm wavelength ranges (where the hot corona gives a negligible background solar radio emission) is given by (6.17). The excess of brightness for the x-mode above the o-mode is

$$\Delta T_b = T_e(\tau_x = 1) - T_e(\tau_o = 1) \; . \tag{6.32}$$

At short cm wavelengths a typical value for spectral index from observations (see 6.25) is $n \approx 1$. That implies

$$\Delta T_b / T_b \approx \Delta\nu / \nu \; . \tag{6.33}$$

So, according to (6.29), the sensitivity to the magnetic field in this case is approximately a factor of two lower than in the case of transparent coronal structures.

The magnetic field in the case under consideration can be found from (6.29). In this case we also need to use spectral observations to find the spectral index n (see 6.25). This reflects the level of the gradient of temperature in the emitting layer, mostly at the depth of $\tau = 1$. At the short cm waves for the quiet Sun, $n \approx 1$. For better accuracy n certainly should be measured simultaneously with the degree of polarization.

In contrast with the previous case of coronal condensations the magnetic field measured in the chromosphere refers to a rather thin layer defined by (6.17). So the approximation of homogeneous magnetic field seems to be reasonable. Below we illustrate this method in the chromosphere of ARs (see §6).

An interesting point in the case under consideration is that the presence of the magnetic field may produce a polarized component without significant spatial variation of total intensity. The reason is that the presence of a magnetic field shifts the effective emitting level for the two modes (two circular polarizations) in different directions: the x-mode becomes optically thick in hotter, higher levels of the solar atmosphere, while the o-mode comes from lower cooler levels.

4.3 Combination of optically thin and thick regions

This situation is quite common when we observe a bright source on the disk that is due to the emission of some condensation of coronal material. For short cm waves it is usually optically thin. This can be checked from an analysis of the spectrum in the intensity channel, which may be dominated by the almost flat chromospheric spectrum. The polarized flux in this situation, however, may be significantly affected by both emission of the condensation and the lower opaque solar atmosphere (chromosphere levels). This may be checked by spectral observations. If the polarized emission T_b^V does not follow the law

$$T_b^V = \frac{1}{2}(T_b^R - T_b^L) \propto \lambda^3 \ , \tag{6.34}$$

then it is significantly affected by both emissions.

However, the spectral observations may help to solve the problem and allow the effective magnetic fields to be found separately for the chromosphere below the radio source and that in the coronal condensation. The observed brightness temperature is the sum of the cold background and hot but transparent region in the overlying corona.

$$\begin{aligned} T_b^I(\lambda) &= T_{b,chr}^I(\lambda)(1-\tau_1\lambda^2) + T_e\tau_1\lambda^2 \\ T_b^V(\lambda) &= T_{b,chr}^V(\lambda)(1-\tau_1\lambda^2) + T_e\tau_1\lambda^2 \cdot 2\lambda/\lambda_B \ . \end{aligned} \tag{6.35}$$

To a reasonable approximation these equations can be written in the following forms. For the intensity:

$$T_b^I(\lambda) = T_1 \cdot \lambda^n + T_2 \cdot \lambda^2 \tag{6.36}$$

and for the circular polarization:

$$T_b^V(\lambda) = T_1 \cdot \frac{\lambda^{n+1}}{\lambda_B^{chr}} + T_2 \cdot \frac{\lambda^3}{\lambda_B^{cor}} \ . \tag{6.37}$$

Equation (6.36) can be used to find parameter n from spectral observations, reflecting the gradient of temperature in the emitting layers of the chromosphere. Then (6.37) gives as the value of λ_B, equivalent of magnetic field,

based on polarization measurements. In this case the longitude component of the magnetic field strength is

$$B_l = \frac{10800}{\lambda_B} \ . \tag{6.38}$$

This can be found from spectral polarization observations separately for the chromosphere λ_B^{chr} and corona λ_B^{cor}.

5. Radio Magnetograms of Solar Active Regions

At short cm waves the radio emission of an active region is mostly generated by thermal mechanisms outside of flaring periods. The magnetic field at the level of the upper chromosphere and the CCTR can be deduced, as has been shown above using (6.29). The radio observations made at the RATAN-600 in the wavelength range of 2–4 cm with the high one-dimensional resolution demonstrated effectiveness of the method on an example of a flocculus (Bogod & Gelfreikh 1980). The magnetic field of about 50 G was measured with the accuracy of about 10 G, the latter being in good agreement with the optical observations. The spectral index in the range of $n = 0.7$–1.0 was found for the flocculus region.

The most effective radio magnetography of solar ARs today is based on the Nobeyama Radioheliograph observations at $\lambda = 1.76$ cm (Shibasaki *et al*. 1994), where both intensity and circular polarization maps are regularly obtained with 2D resolution of about 15 arc sec. Two mechanisms of the generation of the thermal radio emission should be taken into account—gyroresonance (or cyclotron) emission and bremsstrahlung. From numerous modeling computations one knows that the emission at the third and second harmonics of the electron gyrofrequency plays the main role in the observed radio emission of ARs (see Chapter 5). For $\lambda = 1.76$ cm, the second and third harmonics of the electron gyrofrequency correspond to magnetic field strengths of 2000 and 3100 G, respectively.

It is clear that a gyroresonance radio source can be observed with Nobeyama only above sunspots in which strong magnetic fields of $B \approx 2000$ G penetrate into the corona (3100 G needed for the second harmonic is a very rare case). In any case, emission at the third harmonic of the gyrofrequency is strongly polarized, so such radio sources are easy to identify and consider separately.

To measure the magnetic field, we use (6.29). It follows that besides measurements of degree of polarization, which we can get from the I and V radio maps of Nobeyama, we need also some spectral observations in order to measure the spectral index n in (6.25). This is certainly the main limitation of the Nobeyama Radioheliograph data. We may try to overcome this difficulty using some approximations/assumptions. If we look at a typical radio map of

an active region (Figure 6.1) we see no significant increase of brightness over most of it. That implies no significant difference exists in the thermal structure of the solar atmosphere at the levels from which we observe the emission. So, as a reasonable approximation we use the same spectral index of about $n \approx 1$ that is known for the quiet Sun and weak plage regions at $\lambda = 1.76$ cm, being in reasonable agreement with the RATAN-600 data (Bogod & Gelfreikh 1980). Next, we use the assumed value for the Nobeyama brightness temperature for the quiet sun $T_b \equiv 10^4$ K. Using these approximations we can see that (6.29) becomes simply

$$B_l = \frac{107}{\lambda} \frac{V}{I} \times 100 \approx T_b^V \ . \tag{6.39}$$

From this relation one can conclude that V radio maps of the Nobeyama radio heliograph can be used directly as approximate magnetograms of the active regions. So, we have come to a possible method of simple and effective magnetography of the ARs using Nobeyama radio heliograms.

The next problem we deal with is that of sensitivity. The most often used time averaging at Nobeyama is 10 s—just such maps in FITS format are accessible from Nobeyama. The sensitivity of these is about 1% and, according to (6.39), the accuracy of such magnetograms is about 100 G. That is not very good for our goal. However, we can improve our sensitivity by using longer averaging of the images, say for 10 min instead of 10 s. An example of the resulting magnetogram of an active region is shown in the Figure 6.1.

To check the extent to which the method leads to reasonable results, we compared the radio magnetogram with the optical one, averaged with the beam pattern of the radio heliograph (see Figure 6.1). For this case and some others the results seem to be in reasonable agreement, not only in structure but in the values of the magnetic field strength as well (Gelfreikh & Shibasaki 1999).

On all the magnetograms we can clearly see the sunspots as the regions of the highest degree of polarization (some tens of percent). The polarized signal in this case, however, did not show such good correlation with the strength of the magnetic field of the spot (at photospheric level).

6. Magnetic Fields in Prominences

The physics of prominences plays an important role in modern understanding of all types of solar activity because they reflect the position of the neutral lines of the photospheric magnetic field, both in its global and local AR structures. In the latter case it represents the location of the highest flare activity. The complicated plasma and magnetic structure of the surrounding regions is of great interest for studying the nature of the solar flares and other processes of the solar energy release.

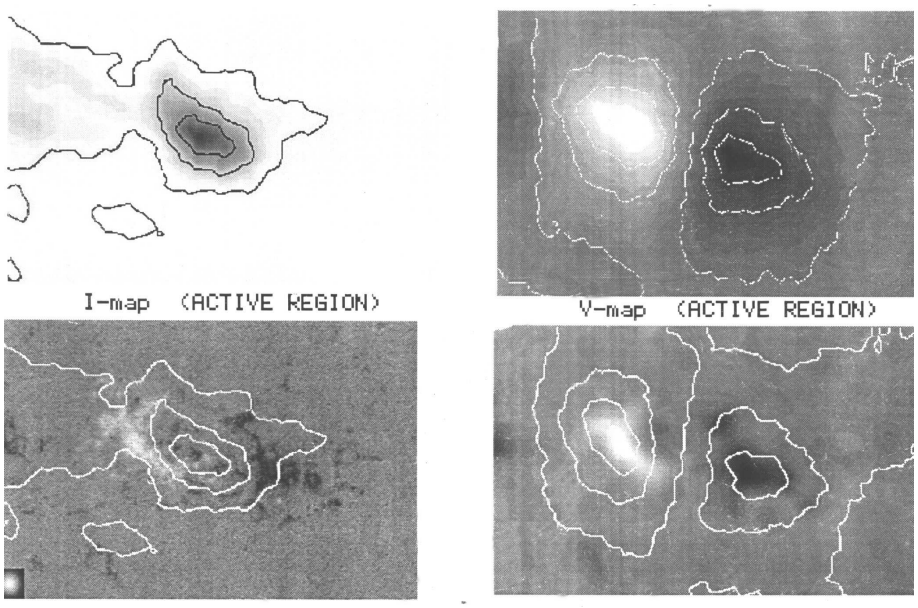

Figure 6.1. Radio maps of the AR observed on June 09, 1995 using Nobeyama radio heliograph at $\lambda = 1.76$ cm. Contours present the brightness distribution . Maximum in I channel ($T_b = 27 \cdot 10^3 K$). Maximum in V-channel $T_b^V = 440K$. Maximum degree of polarization $P = 2.8\%$. The region maps are overlapped by gray scale magnetograms . For V-maps they are averaged by the scale of the Nobeyama radio heliograph beam (shown below on the left). The upper V-map present brightness T_b^V , the lower one—percentage $P\%$ of polarization.

Radio observations of free-free emission offer a new method of measuring the magnetic field inside prominences, though at present the combination of spatial and spectral resolution of the radio observations is not sufficient for detailed study. Measurements of the prominence magnetic fields have been made using the 22 meter dish RT-22 of the Crimean Astrophysical Observatory at the wavelengths of 8 and 13.5 mm. A dozen prominences were analyzed in 1993 (Apushkinsky *et al.* 1996). The longitudinal component of the magnetic field was found to be in the range from 7 to 30 G, depending on the prominence. This result is in reasonable agreement with the optical data. The maximum value of the field usually was found at higher regions within the prominences, where in fact one can expect the maximum of the longitudinal component.

A similar conclusion, but with stronger magnetic field, was found with the RATAN-600. In figure 6.2 we see a one-dimensional scan of the limb of the solar disk at wavelength $\lambda = 2.1$ cm, both in intensity and circular polarization. The quiet Sun level has already been subtracted. The bright source behind the west limb is due to the prominence and surrounding plasma structures in the

solar corona (at $\lambda = 2.1$ cm they are weak). The maximum polarization signal $P = (6 \pm 1)\%$ coincides with the upper part of the prominence where probably the plasma is already optically thin. The resulting magnetic field we get is $B_l \approx 150 \pm 25$ G. This field is an order of magnitude higher than in the previous case based on observations made with the RT-22. One possible reason is due to the higher resolution of the RATAN-600. Alternatively, it may be due to a stronger AR in which the prominence appeared.

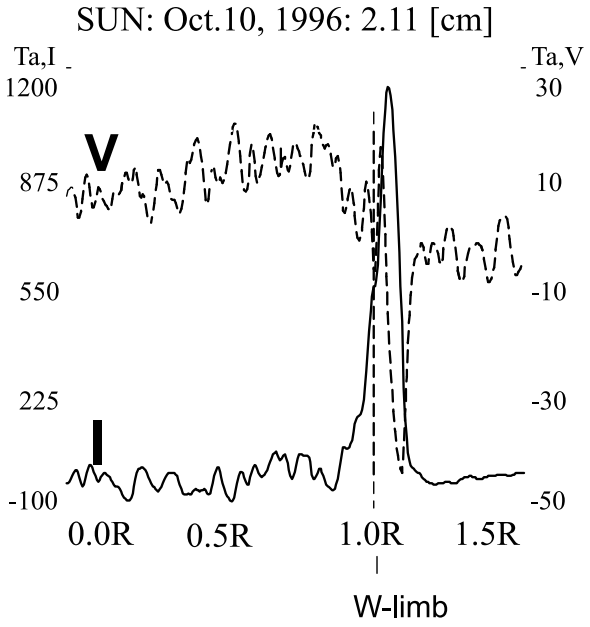

Figure 6.2. Radio scan of the prominence at a wavelength $\lambda = 2.1$ cm made with the RATAN-600 on 1996 October 11. Intensity (I) and circular polarization (V) are shown. The level of the quiet Sun has been excluded from the intensity curve. The upper part of the prominence is polarized: $P = (6 \pm 1)\%$

7. Magnetic Fields in a Coronal Hole

The coronal holes (CH) are important structures of the solar corona both from the point of the solar activity and the nature of plasma structures. They are known to be the regions of acceleration of fast geoeffective solar wind. They are the regions of lower density and temperature as well as the lower gradient of temperature in the transition region. They reflect open magnetic field structures, unlike the closed-field regions of the surrounding solar atmosphere.

The CHs are directly observed in soft X-rays and EUV from space. In the ground-based observations they are identified mostly in the He I line 10830 Å

(the "reflections" in the chromosphere). At the limb CHs are clearly identified in the green coronal line. As far as the radio observations are concerned they appear as dark regions at dm wavelengths (see figure 6.3). At short centimeters the input emission of the corona is too weak and at meter waves the large optical thickness of the corona smoothes the effect.

As follows from (6.9) and (6.20), in the case of optically thin emission the brightness $T_b \propto n_e^2/\sqrt{T_e}$. So, it only slightly depends on the coronal temperature, and the lower electron density in the CH produces the main contrast observed on a radio map. The brightness depression really amounts to some tens of percent but for measurements of magnetic field we must detect some much smaller polarization effects, which are accessible only to a few of the largest instruments in the world. We could expect magnetic field in the corona of a CH to be of the order of 10 G or even lower (the CH are generally observed outside the solar ARs). For $\lambda \approx 30$ cm this would result in degree of polarization of $P \approx 2\%$ (see 6.28), implying the necessary sensitivity of the instrument to polarization measurements of about 0.1%.

In fact, at present only one case of publication of the radio measurements of the magnetic fields in a CH is registered (Borovik *et al.* 1999). The observations have been carried out with the reflector radio telescope RATAN-600. Figure 6.3 illustrates the observations of a coronal hole made with the RATAN-600. Observations of the same CH in EUV (line FeXII 195 Å) is also presented. From the Figure 6.3 it is clearly seen that the CH is well registered at dm wavelengths ($\lambda \geq 10$ cm).

The magnetic field strength (averaged longitudinal component) was found from (6.29) using the observations made with the radio telescope RATAN-600. The logarithmic spectral index n was found as a function of wavelength (see 6.25): $n = 0.9$ at 9–11 cm, $n = 1.04$ at 14–18 cm and $n = 1.7$ at 27–30 cm (measured on October 12, 1996). The magnetic field strength in the CH according to expression above is presented in Figure 6.4. Taking into account the magnetic field measurements at the photosphere level (Stanford data) we have concluded that the longitudinal component of the magnetic field in the coronal hole increases with height from 0.2 G at the photospheric level to 7–10 G at the level of the generation of radio emission at 18 cm. In this wavelength range practically all of the emission is due to coronal plasma and the obtained value of B_l is a mean one weighted by the distribution of n_e^2. At shorter wavelengths, a contribution from the chromosphere is expected. That implies a lower strength of the field in the chromosphere-photosphere level, in good agreement with the optical data.

One can hope that the problem of the 3D-structure of the magnetic field in coronal holes and related solar wind acceleration phenomena may be successfully resolved using radio astronomical instruments providing both high spatial resolution and high sensitivity for polarization measurements. Spectra

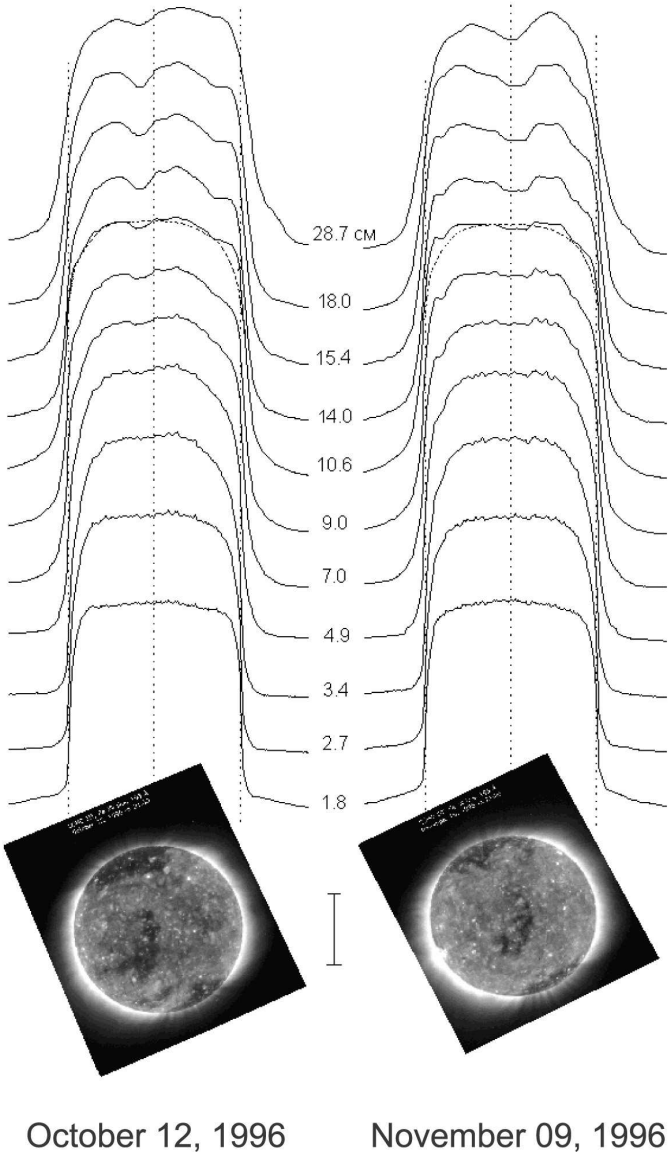

Figure 6.3. One-dimensional radio scans of the sun made with the RATAN-600 at eleven wavelengths in the range 1.8–28 cm for 1996 Oct 12 and Nov 9. Coronal holes are seen as brightness depressions at dm waves. For identification of the CHs at the bottom the EUV maps of the Sun (SOHO data) are shown.

at the short cm wavelengths in this case could be used for magnetography at the chromospheric level.

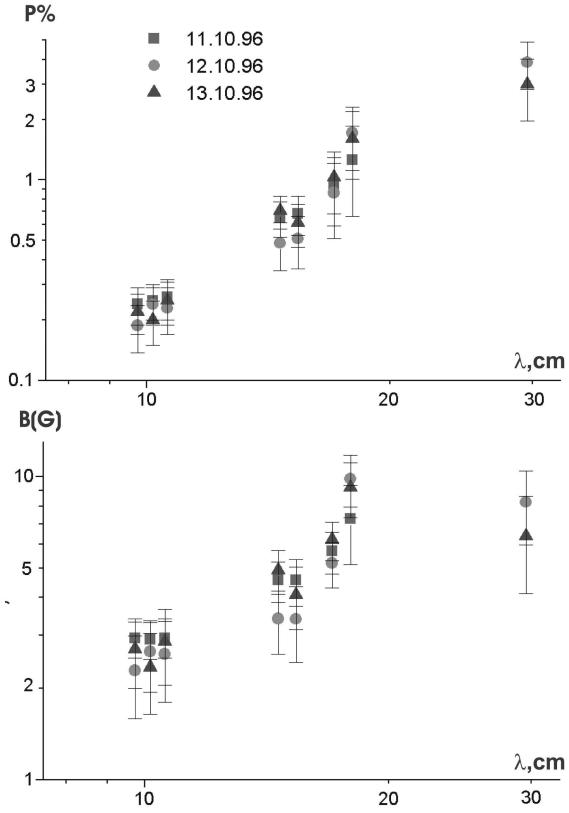

Figure 6.4. Percentage of circular polarization (upper curve) and effective value of the magnetic field (lower curve) for the coronal hole obtained from observations made with the RATAN-600. The observations were made on 1996 October 11, 12, 13.

8. Magnetic Fields in Coronal Loops

As we have discussed already for an optically thin plasma the emissivity for the thermal bremsstrahlung $\eta \propto n_e^2/\sqrt{T_e}$ (see 6.9). So, the emission is heavily weighted to high density regions in the solar corona and the radio maps are expected to reflect any type of plasma structures in the upper parts of the solar atmosphere. In contrast to the solar images obtained in the EUV lines, e.g. obtained with SOHO, the radio emission is weakly ($\propto T^{-1/2}$) dependent on the electron temperature. The longitudinal component of the magnetic field in this case is found using (6.28) based on polarization measurements. It represents the averaged value of the field weighted by n_e^2. We illustrate the method with

an example of a coronalarch (Figure 6.5) observed on the disk and connected with the CME (Borovik *et al.* 2002).

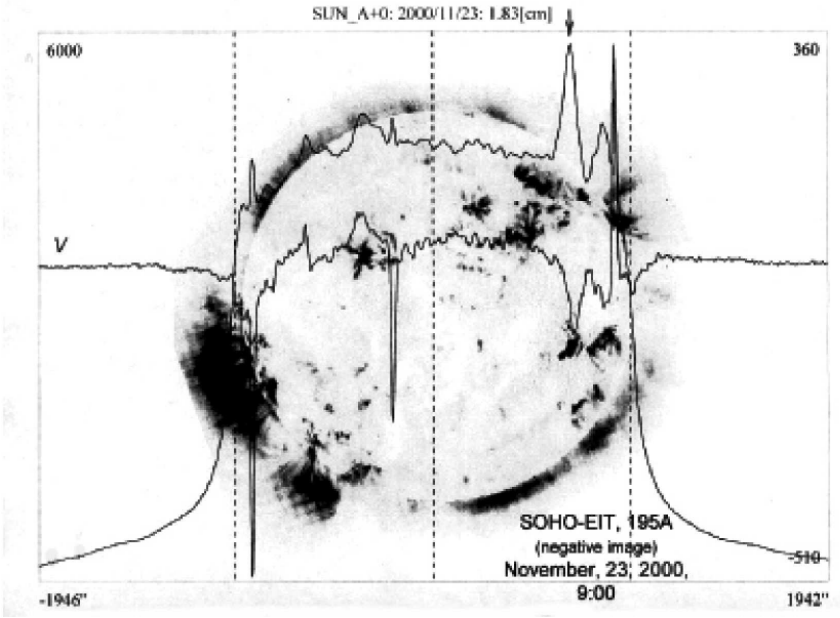

Figure 6.5. Radio scans of the Sun on 2000 November 23. The observations at the wavelength $\lambda = 1.8$ cm in intensity (I) and circular polarization (V) were made with the RATAN-600. The bright region at 195 Å according the SOHO data are shown for comparison. The coronal loop connected with the CME is marked by an arrow.

From the spectra presented at the Figure 6.6 one can conclude that the emission is really produced by the thermal bremsstrahlung from an optically thin coronal structure. The corresponding magnetic field strength was found in the range of 200–250 G. Similar values for the same structure were found from the Nobeyama radio heliograph data. An increase of the field from 150 to 200 G was registered, probably connected with the CME event. The next day the source of the coronal arch disappeared.

9. Future Development of the Method

The examples above demonstrated high effectiveness of the method of measuring magnetic fields in the solar chromosphere and corona based on analysis of bremsstrahlung radio emission. These include such coronal structures as prominences, coronal holes, CMEs, loops, and arches. The potential sensitivity of the method exceeds 1 G. The magnetic fields of few gauss in the corona have already been reported using the RATAN-600 spectral-polarization

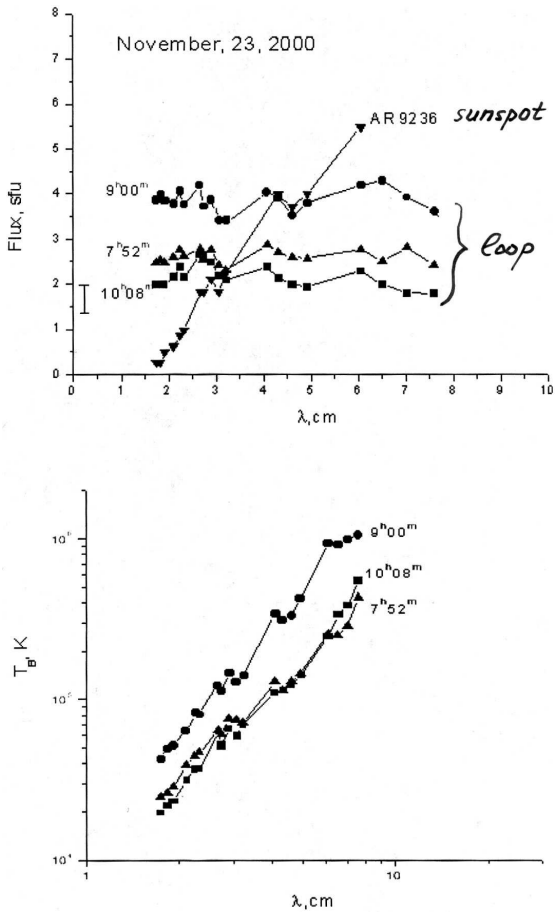

Figure 6.6. The spectra of the radio emission of the CME-associated coronal loop obtained with the RATAN-600 on 2000 November 23 for three times. The upper curves represent the spectra of intensity. For comparison also a spectra of the sunspot-associated source is shown. At the bottom, the spectra of brightness for the same loop are shown.

observations. In contrast to the method based on the observations of the gyroresonance emission (see Chapter 5, by White), the bremsstrahlung method is applicable to measurement of weaker magnetic fields (see Chapter 4, by Gary & Hurford), and presents an average of the longitude component of the field weighted by n_e^2.

In comparison with the method based on the observation of the inversion of the sign of the circular polarization (chapter 7) bremsstrahlung does not require a special region of quasi-transverse propagation and, being comparable in sensitivity, may have more general applications.

However, the method under discussion needs much higher sensitivity for polarization analysis and some spectral observations. So, at the moment numerous structures were accessible only to observations made with the instrument of high collecting area—RATAN-600. Stronger magnetic fields in active regions could be analyzed using the modern radio heliograph at Nobeyama, resulting in 2D radio magnetography. The future development of these approaches, using a combination of high spatial and spectral resolution, may give a new observational basis for the theory of the solar plasma. This is of great scientific interest because most of the energetic processes in the corona are directly due to the interaction of magnetic structures, and no other means to measure magnetic fields in the corona are available.

Acknowledgments

The results presented in this chapter were partially made with the support of the grants of the RFBR 02-02-16548 and INTAS 00181.

References

Apushkinsky, G. P., Tochilo, N. A., Tsyganov, A. N. & Nesterov, N. S. 1996, Astron. Nachr. 317, No. 6, 317

Benz, A. O. 1993, Plasma Astrophysics, Kluwer Academic Publishers.

Bogod, V. M. & Gelfreikh, G. B. 1980, Solar Phys, 67, 29

Bogod, V. M., Grebinskij, A. S. & Garaimov, V.I. 1998, Solar Phys, 182 139

Borovik, V. N., Medar, V. G. & Korzhavin, A. N. 1999, Astronomy Letters, 25, No.4, 250

Borovik, V. N., Gelfreikh, G. B., Medar, V. G. & Grigorieva, I. Y. 2002, Proc. 10th European Solar Physics Meeting, (Noordwijk: ESA Publ.), ESA SP-506, 431

Brosius, J. W., Davila, J. M., Thomas, R. J. & White, S. M. 1997, ApJ, 488, 488

Gelfreikh, G. B. 1994, IAU Colloq. 144, (VEDA Publ. Company, Bratislava), 21

Gelfreikh, G. B. 1998, Proc. of Nobeyama Symposium, NRO report No. 479, 41

Gelfreikh, G. B. & Shibasaki, K. 1999, Proc. 9th European Meeting on Solar Physics, ESA SP-448, 1139

Grebinskij, A., Bogod, V. M., Gelfreikh, G. B., Urpo, S., Pohjolainen, S. & Shibasaki, K. 2000, A&A Suppl., 144, 169

Shibasaki K., Enome S., Nakajima H., Nishio M., Takano T., Hanaoka Y., Torii C., Sekiguchi H., Kavbashina S., Bushimata T., Shinchara N., Koshiishi H., and Shiomi Y. 1994, Proc. Kofu Symposium, NRO Report No. 360, 45